JOURNAL OF SOLID STATE CHEMISTRY **139,** 27–36 (1998)
ARTICLE NO. SC987787

Temperature- and Gaseous Phase-Mediated Reorganization and Paramagnetic Doping of Solid Aluminum Fluorides: ESR and *ab Initio* Quantum Chemical Studies

G. Scholz

Humboldt University of Berlin, Institute of Chemistry, Hessische Str. 1-2, D-10115 Berlin, Germany

Received July 8, 1997; in revised form December 22, 1997; accepted February 6, 1998

Based on cw-X-band ESR spectroscopic measurements of Mn^{2+} doped AlF_3 powder samples and DFT(B3LYP)/6-31+G* quantum chemical calculations it is shown that structural reorganization of AlF_3 (AlF_3 (amorphous) → AlF_3 (crystalline)) are necessarily assisted by chemical reactions with the participation of water.

It could be unambiguously demonstrated that Mn^{2+} ions are suitable spin probes for reorganization processes from amorphous to local crystalline regions in fluoride matrices. The resolution of the ^{55}Mn–^{19}F– superhyperfine structure (both the formation of regular MnF_6^{4-}– species as well as the reduction of strain effects by transformation of the amorphous parts) is a sensitive indicator of the formation of local crystalline regions.

DFT(B3LYP)/6-31+G* calculations of $(AlF_3)_n(H_2O)_m$ complexes (n: 1,2; m: 1–3) resulted in first and acceptable ideas of structures, energetical stabilities, and vibrational frequencies of hydrated AlF_3. The calculated strength of the Al–O bond, resulting in the stable $\{AlF_3$–$OH_2\}$ subunit, and the favored splitting of Al–F–Al bonds by H_2O molecules, are the main reasons for the immediate and spontaneous hydration of freshly prepared amorphous AlF_3. Independent of the size of the model complexes, stable substructures like $\{AlF_3$–$H_2O\}$ and $\{F_3AlFAlF_2$–$OH_2\}$ can be recognized in all optimized structure models. © 1998 Academic Press

1. INTRODUCTION

Properties directly related to the function of Al–F– and Al–O– compounds as chemical agents, catalysts, or materials can be significantly changed by doping or transformation of the matrices into nonequilibrium states. Although many empirical facts and theoretical attempts are available in the literature concerning the preparation and characterization of such active system (1), the knowledge about the effects of an interacting gaseous phase in such structural and electronic reorganization processes is rather marginal. Inspecting, for example, solid fluorides of aluminum, interesting facts can be extracted from experimental findings. Obviously, transitions between crystalline and amorphous phases of aluminum fluorides underlie the combined action of defect-chemical processes and gaseous intermediates (2). This is supported by thermal techniques using Q-crucibles (2b–2d), which guarantee quasi-isobar conditions and yield, as empirically demonstrated, sufficiently good conditions to obtain crystalline products at thermal decompositions. A further experience concerns the difficulty of separating Mn impurities from solid Al–F– compounds by sublimation. It proves to be a tedious task because of the formation of the stable gaseous $MnAlF_5$ complex (3). The existence of this complex can be proven experimentally by coupled thermoanalytical/mass spectroscopic measurements, and can be supported by ab initio calculations (3). Otherwise, $MnAlF_5$ formed in the gas phase can be used as a doping agent at the vapor deposition of AlF_3-containing Mn^{2+}–point defects. Intermediates should play a *key* role at the sublimation of AlF_3 as well as the cocondensation of gaseous species (e.g., $AlF_3 + MnAlF_5$ (3)) to form doped solids like AlF_3/M^+.

Until now, the advantage of a localized or even molecular approach to understanding reorganization and doping processes has not been explored for the systems mentioned above. In particular, there has been no exploration of the dependence of these processes on the gaseous atmosphere and especially on the available p_{H_2O}. First attempts to model hydration processes of aluminum fluorides and chlorides at a molecular level have been published recently (4). Quantum chemical ab initio calculations have been performed using Hartree-Fock (HF), Moller-Plesset (MP2), and density functional (DFT) methods for the complexes AlX_3–OH^-, AlX_3–H_2O, AlX_3–$2H_2O$, and AlF_3–$3H_2O$ (X: F, Cl), which were found to be energetically stable (4).

In this paper the interest is focused first on the findings of ESR investigations performed in combination with X-ray diffraction, infrared, and thermoanalytical methods on doped aluminum fluorides AlF_3/Mn^{2+}. Mainly based on local spectroscopic information, these experiments indicate

0022-4596/98 $25.00

the first steps of water-mediated reorganization of the solids. Although the ensemble of methods applied sensitively indicates electronic and geometrical changes related to reconstruction processes, it is very difficult to get *direct* evidence of intermediates formed by reactions of water traces with the AlF_3 matrix. A very promising way out is a theoretical approach, which provides unique knowledge concerning structural and energetic properties of probable intermediates.

Therefore, a series of quantum chemical *ab initio calculations* have been performed to discover the most probable structures of intermediates formed by reactions of AlF_3 with water molecules. In particular, the complexes $(AlF_3)_n \cdot (H_2O)_m$ (n: 1,2: m: 1,2,3) were taken into account. Together with the structures, the corresponding energies, reaction enthalpies[1] including corrections for the BSSE[2], zero point vibrational energies, and vibrational frequencies were determined.

It is the unusual combination of the results of a local spectroscopic method with those of molecular quantum chemical calculations which is expected to give a deeper and special insight into the solid state chemical and reconstruction processes. Based on a variety of experimental and theoretical results available today, an actual hypothesis concerning these solid state processes was formulated. It is the aim of the present paper to verify this hypothesis by ESR and quantum chemical investigations: The structural reorganization of AlF_3 proceeds by thermal energy and is necessarily assisted by chemical reactions of the solid with traces of water. This process includes as a key reaction the formation of intermediates with strong Al–O– bonds. A second key reaction concerns the cleavage of two fluoride bridges (–Al–F–Al–) by at least three water molecules. Both of the reactions mentioned can occur with the participation of fluorides in the gaseous or the solid state. Favored by their energetical low-lying ground states, the substructures $\{AlF_3–OH_2\}$ and $\{F_3Al–FAlF_2–OH_2\}$ appear to be especially relevant chemical intermediates occurring at the transformation AlF_3(amorphous) $\rightarrow$ AlF_3(crystalline). The driving force for this reorganization process originates from progressive local activation by alternating hydration/dehydration processes with the participation of water traces.

2. METHODS

Previous studies of the complexes $AlX_3–H_2O$, $AlX_3–2H_2O$, and $AlF_3–3H_2O$ (X: F, Cl) using Hartree-Fock (HF), Møller-Plesset (MP2), and density functional (DFT) methods have shown (4) that DFT(B3LYP) calculations in combination with the 6-31+G* basis set yield BSSEs of less than 10% of the complex binding energies. This indicates a proper choice of the basis set applying this method. Moreover, the calculated harmonic vibrational frequencies are quite reliable at the DFT(B3LYP)/6-31+G* level in comparison with MP2/6-31+G* and MP2/6-311G** results (4). Therefore, the calculations of $(AlF_3)_n \cdot (H_2O)_m$ (n: 1, 2; m: 1–3) complexes presented in this paper were only performed at the DFT(B3LYP)/6-31+G* level (5). This ensures qualitatively accurate results including electron correlation effects at relatively low computational costs even for the larger complexes. The optimizations of geometries were performed without limitations for the symmetry if not otherwise indicated. All quantum chemical calculations have been carried out with the GAUSSIAN 94 (6) program on IBM RS6000 and HP9000/735 workstations as well as on a CRAY YMP 4D/464 computer. The vapor deposition of Mn^{2+}-doped AlF_3 was realized using (i) the evaporation equipment B30.2 (Fa. Hochvakuum Dresden, Germany) combined with a target movable in two dimensions, and (ii) directly in ESR quartz tubes connected with a high-vaccum apparatus (Fa. Leybold, Germany) located in a horizontal furnace as described in Ref. (7). Various target temperatures and partial pressure of water were used for evaporation and condensation processes under a vacuum atmosphere. Mixtures of pure, water-free α-AlF_3 with MnF_2 (10^{-2} mol% MnF_2) were used as starting materials.

The cw-ESR measurements were carried out at 77 and 298 K with the X-band spectrometer ERS300 (Center of Scientific Instruments, Berlin-Adlershof, Germany). Simulations of the powder spectra were performed by diagonalization of the full spin-Hamiltonian matrix (8), applying an appropriate spin Hamiltonian for the $S = 5/2$ and $I = 5/2$ problem of Mn^{2+}.

Furthermore, changes of the solid matrix during hydration/dehydration processes have been observed by X-ray diffraction methods (HZG-4C, Präzisionsmechanik Freiberg, Germany) and by the application of the FT-IR microscopy (Mattson GL 5020 FT-IR spectrometer).

3. EXPERIMENTAL RESULTS

Figure 1 depicts typical X- and Q-band spectra of Mn^{2+}-doped crystalline α-AlF_3, which are characterized by very well-resolved $^{55}Mn–^{19}F–$ superhyperfine structures.

Amorphous AlF_3 doped with Mn^{2+} ions was obtained by chemical vapor deposition, starting from a mixture of crystalline α-AlF_3 with MnF_2. Figure 2a shows the typical ESR spectrum of amorphous AlF_3/Mn^{2+} deposited at a target with temperature $T = 200°C$ in the evaporation equipment. The spectrum is characterized by six ^{55}Mn–hyperfine transitions with a hyperfine coupling constant A_{Mn} of 9.8 mT, which was determined by simulation (Fig. 2b). The experimental resonance positions of the hyperfine transitions exhibit a remarkable dependence on the magnetic field

[1] For a temperature of 0 K.

[2] BSSE: basis set superposition error.

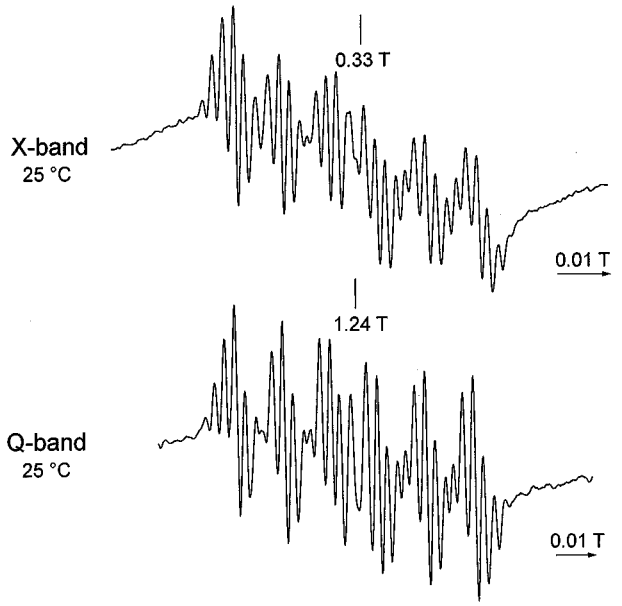

FIG. 1. Experimental X- and Q-band ESR spectra taken at 298 K of Mn^{2+} doped α-AlF_3. The sample was obtained as result of thermoanalytical quenching of β-$AlF_3 \cdot 3H_2O/Mn^{2+}$ at 800°C; $A_{Mn} = 9.8$ mT (hyperfine coupling constant), $A_F = 2.45$ mT (^{55}Mn–^{19}F– superhyperfine coupling constant); ESR intensities in arbitrary units.

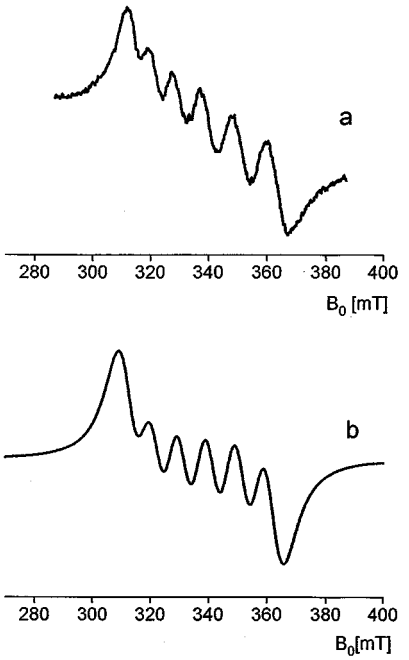

FIG. 2. (a) X-band ESR spectrum (293 K, $P_{MW} = 50.2$ mW) of sublimated AlF_3/Mn^{2+} deposited at a target with $T = 200$°C (ordinate: ESR intensities in arbitrary units; and (b) Simulated X-band ESR spectrum of Mn^{2+} doped AlF_3, parameters: $S = 5/2$, $I = 5/2$, $g = 2.0$, $A_{Mn} = 9.8$ mT, $a = 9.8$ mT, $\Delta B_i = 4$ mT.

which results from both fine structure contributions and hyperfine effects of higher order. In contrast to Fig. 1, no ^{55}Mn–^{19}F– superhyperfine splitting could be resolved for the amorphous state. The same value of ^{55}Mn–hyperfine coupling constant, 9.8 mT (Fig. 2), as observed for the crystalline state (cf. Fig. 1) justifies the assumption of the existence of fluorine-coordinated Mn^{2+} ions even in the amorphous state. Obviously, the distribution of the spin-coupling parameters in the amorphous state prevents the resolution of the superhyperfine structure. All of these findings, along with the large line widths, make the observed ESR spectra of vapor-deposited amorphous AlF_3/Mn^{2+} very similar to those of Mn^{2+} point defects in heavy metal fluoride glasses (9)[3]. Samples obtained by sublimation are colorless, transparent, glass-like, and do not stick well to the target. X-ray powder diffraction examinations underlined the amorphous nature of the sublimate (7).

The assumption that amorphous AlF_3 has pronounced hygroscopic properties compared to crystalline α-AlF_3 can be verified by the application of mass spectroscopy and FT-IR microscopy. The release of H_2O and HF was indicated by mass spectroscopy after heating the amorphous sample to 300°C. FT-IR microscopic measurements of amorphous as well as crystalline samples clearly demonstrated the hydration of amorphous AlF_3, at least in the surface region (cf. Fig. 3). Even freshly prepared amorphous AlF_3 shows nearly the same spectral IR-pattern as crystalline α-$AlF_3 \cdot 3H_2O$ after contact with air. Broad IR bands of free and hydrogen bridged OH-groups (ν_{OH}: 3000–3500 cm^{-1}) and of the deformation vibration δ_{HOH} of water molecules at about 1600 cm^{-1} (Fig. 2) are the main characteristics.

Detection of local hydration/dehydration–induced reorganization processes by ESR spectroscopy requires suitable spin probes for a sensitive indication of local changes, e.g., from amorphous to crystalline regions. ESR spectra (Fig. 4) and X-ray powder spectra (Fig. 5) demonstrate that Mn^{2+} ions, interacting with the surrounding ^{19}F nucleii, are qualified as spin probes for such purposes. ESR spectra depicted in Fig. 4 point to an improved resolution of the ^{55}Mn–^{19}F–superphyperfine structure of sublimated AlF_3/Mn^{2+} with increasing target temperatures. This is of special interest, since the value of the ^{55}Mn–^{19}F coupling only amounts to $\sim$2.4 mT as obtained for the crystalline sample (Fig. 1). The typical spectral pattern of amorphous AlF_3 doped with Mn^{2+} ions is retained up to target temperatures of about 200°C. The first signs of the ^{55}Mn–^{19}F–shf coupling can be observed at 400°C (Fig. 4b). At 700°C the ^{55}Mn–^{19}F–shfs is

[3] As in Mn^{2+}-doped fluoride glasses, weak ESR signals at $g' = 4.3$ were observed in amorphous AlF_3. Because the changes of these signals are not significant for the present investigation, they were not included in this paper.

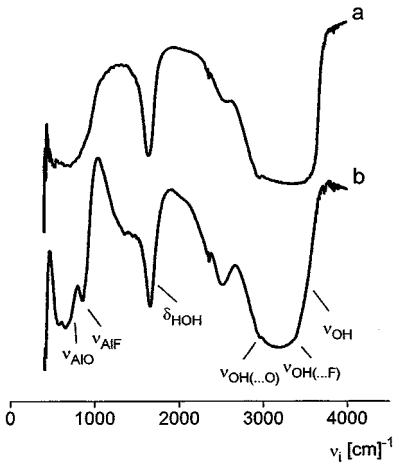

FIG. 3. FT-IR spectra of (a) freshly prepared amorphous AlF_3 exposed to the air and (b) crystalline α-$AlF_3 \cdot 3H_2O$ (ordinate: IR intensities in arbitrary units).

resolved distinctly (Fig. 4d). These results correspond very well with measured X-ray powder diffractograms (Fig. 5). Whereas the amorphous nature of the substrate can be established up to 200°C in addition to the typical Mn^{2+} pattern (Fig. 4a) by the broad basis line of the X-ray powder diffractogram (Fig. 5a), the diffractogram shown in Fig. 5b, with two typical reflexes of crystalline α-AlF_3, points to a growth of regular microcrystals of AlF_3. Obviously, this formation of local crystalline regions can be detected at a microscopic level by observing the incorporation of

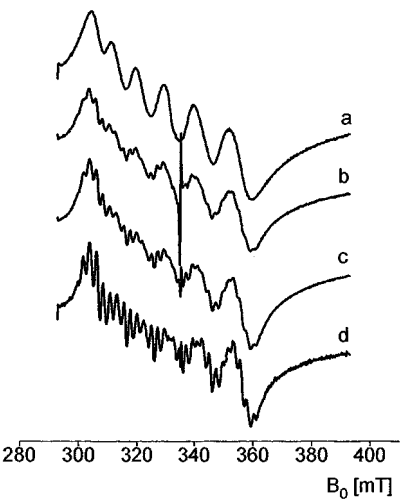

FIG. 4. X-band ESR spectra (77 K) of AlF_3/Mn^{2+} deposited from the gaseous phase at targets with the following temperatures: (a) 200°C, $P = 20$ mW; (b) 400°C, 20 mW; (c) 600°C, 20 mW; (d) 700°C, P = 200 μW. (ordinate: ESR intensities in arbitrary units).

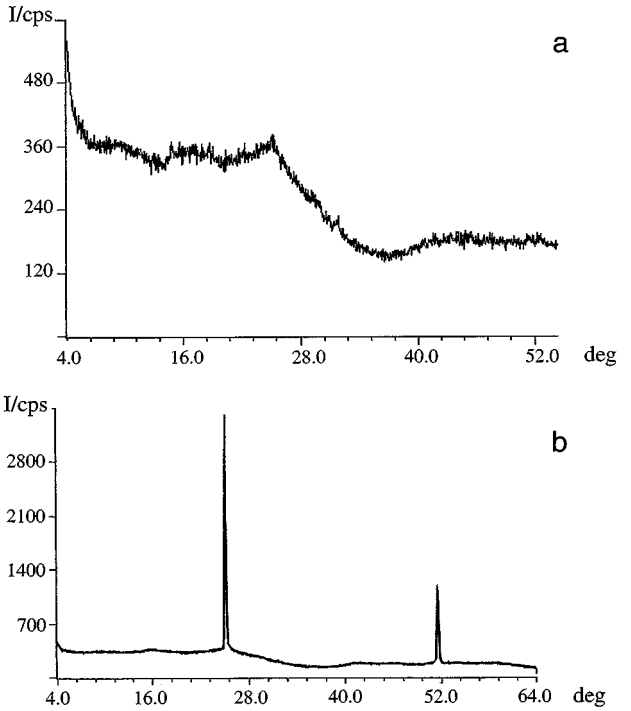

FIG. 5. X-ray powder diffractograms (radiation: Cu$K\alpha$) of AlF_3/Mn^{2+} deposited from the gaseous phase at targets with temperatures (a) 200°C and (b) 400°C. (The line at 42.5° (not observed here) in well-crystallized α-AlF_3 has a substantially lower intensity than the line at 52°. In the present case, the beginning of local crystallization is obviously obscured by the underground.)

Mn^{2+} ions and their magnetic coupling to neighbored F^- ions.

Two key experiments were performed to figure out the roles of the atmosphere and especially the partial pressure of water at the formation of amorphous or crystalline samples. Both vapor deposition processes (as mentioned above) and reorganization of amorphous into crystalline AlF_3 were included in the experiments, starting from a mixure of crystalline α-AlF_3 with MnF_2.

The first study dealt with the vapor deposition of amorphous AlF_3 at several target temperatures and subsequent thermal treatment under vacuum and atmospheric conditions. Figure 6A depicts a series of ESR spectra showing nearly unchanged spectral patterns under varying vacuum conditions (Fig. 6). Only in the case where moisture was available in the air did the thermal treatment lead to first indications of the ^{55}Mn–^{19}F–shfs at deposition temperatures $T \geq 345$°C (Fig. 6B). Again, as depicted in Figs. 4 and 5, the ^{55}Mn–^{19}F–shfs hints at local crystallization effects, which were proven by the distinct formation of two X-ray reflexes of α-AlF_3 (not explicitly shown here; for comparison see Fig. 5b (7)).

In a second key experiment, the vacuum chamber containing amorphous AlF_3 was thermally treated for one hour

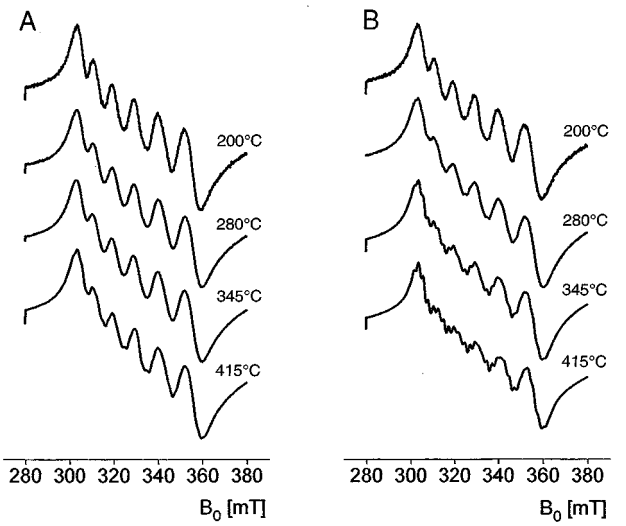

FIG. 6. X-band ESR spectra (77 K, $P_{MW} = 2$ mW) of AlF_3/Mn^{2+}, deposited amorphously at target temperatures given in the figure, and subsequent thermal treatment (a) in vacuum and (b) at the atmosphere (ordinate: ESR intensities in arbitary units).

under an atmosphere of either dry (cf. Fig. 7a) or wet argon (cf. Fig. 7b). Only in the case of available water traces could the ^{55}Mn–^{19}F-shfs be observed accompained by oriented crystal growth (not shown separately here, see Ref. (7)).

4. RESULTS OF AB INITIO CALCULATIONS

As results of HF, MP2, and DFT calculations, the equilibrium structures of AlF_3–H_2O, AlF_3–$2H_2O$, and AlF_3–$3H_2O$ were depicted in Ref. (4) along with the vibrational frequencies of the normal modes of the complexes. It

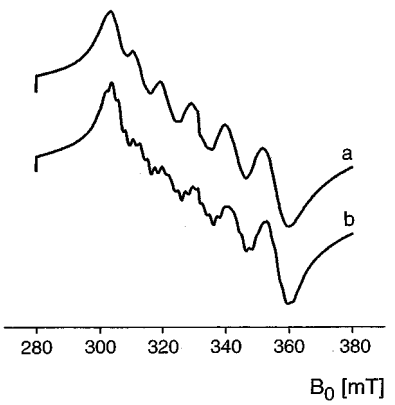

FIG. 7. X-band ESER spectra (77 K, $P_{MW} = 2$ mW) of deposited AlF_3/Mn^{2+} sublimated in (a) dry Ar-atmosphere and (b) wet Ar-Atmosphere, with subsequent thermal treatment for one hour (ordinate: ESR intensities in arbitary units).

became obvious that in all water-containing AlF_3 complexes, the formation of an energetically favored $\{AlF_3$–$H_2O\}$ subunit can be recognized. In this paper, a number of molecular models for complexes between AlF_3 and H_2O molecules could be markedly extended on the basis of previous DFT(B3LYP)/6-31+G* results.

They include structural proposals for AlF_3–$3H_2O$ (3 models), $2AlF_3$–H_2O (5 models), $2AlF_3$–$2H_2O$ (3 models), and $2AlF_3$–$3H_2O$ (until now 2 models); each will be discussed in detail now. All structure models considered in this paper are shown in Fig. 8. The numbers in parentheses indicate the localized stationary points as saddle points of first order (1) or local minima (0) at the potential energy surfaces. The corresponding total and relative energies of all structure models are summarized in Table 1.

The structure models taken into account for AlF_3–$3H_2O$ include the usual fourfold aluminum coordination in the vapor phase as well as a sixfold coordination of aluminum as it appears in most cases in solids. All structures of $AlF_3 \cdot 3H_2O$ depicted in Fig. 8 were found to be local minima at the potential energy surface. The global minimum, represented by structure 1 (C_s), clearly demonstrates the formation of the AlF_3–H_2O subunit interacting with two additional water molecules. Structure 2 (C_1) is only slightly different, caused by rotation of a water molecule around a O–H-axis. Structure 3 (C_1) is energetically clearly discriminated (cf. Table 1).

There are three primary ways to construct a complex consisting of two AlF_3 and one H_2O molecules. These are the formation of: (i) two Al–F–Al– bridges (Fig. 8, structure 6), which means the approach of a H_2O molecule to an Al_2F_6 dimer; (ii) one Al–F–Al– and one Al–O– bond (Fig. 8, structures 4 and 5), which does in fact mean the splitting of the second Al–F–Al– bond of a Al_2F_6 dimer by a water molecule; and (iii) the formation of one Al–O–Al– bridge (Fig. 8, structures 7 and 8), which is equivalent to two isolated AlF_3 molecules interacting with a water molecule.

Among all structure models considered here, the structure 4 (C_1) (Fig. 8) could be assigned to the global minimum at the potential energy surface, energetically followed by structure 5 (C_s), which refers to a first order saddle point. The geometrical equilibrium structure of the global minimum has a cyclic Al–F–Al–O– arrangement with a strong $H \cdots F$ bridge of only 154 pm distance. The cyclic arrangement of the saddle point structure 5 (C_s) consists of two weaker hydrogen bridges of 194 pm each. Two further interesting but energetically discriminated local minima could be obtained starting from two monomolecular AlF_3 units separated by a water molecule (Fig. 8, structures 7 (C_1) and 8 (C_1)). The complex experiences a remarkable stabilization in case of deprotonation of the water molecule, which enlarges therewith the Lewis basicity of the oxygen atom (Fig. 8, structure 8). A conservation of

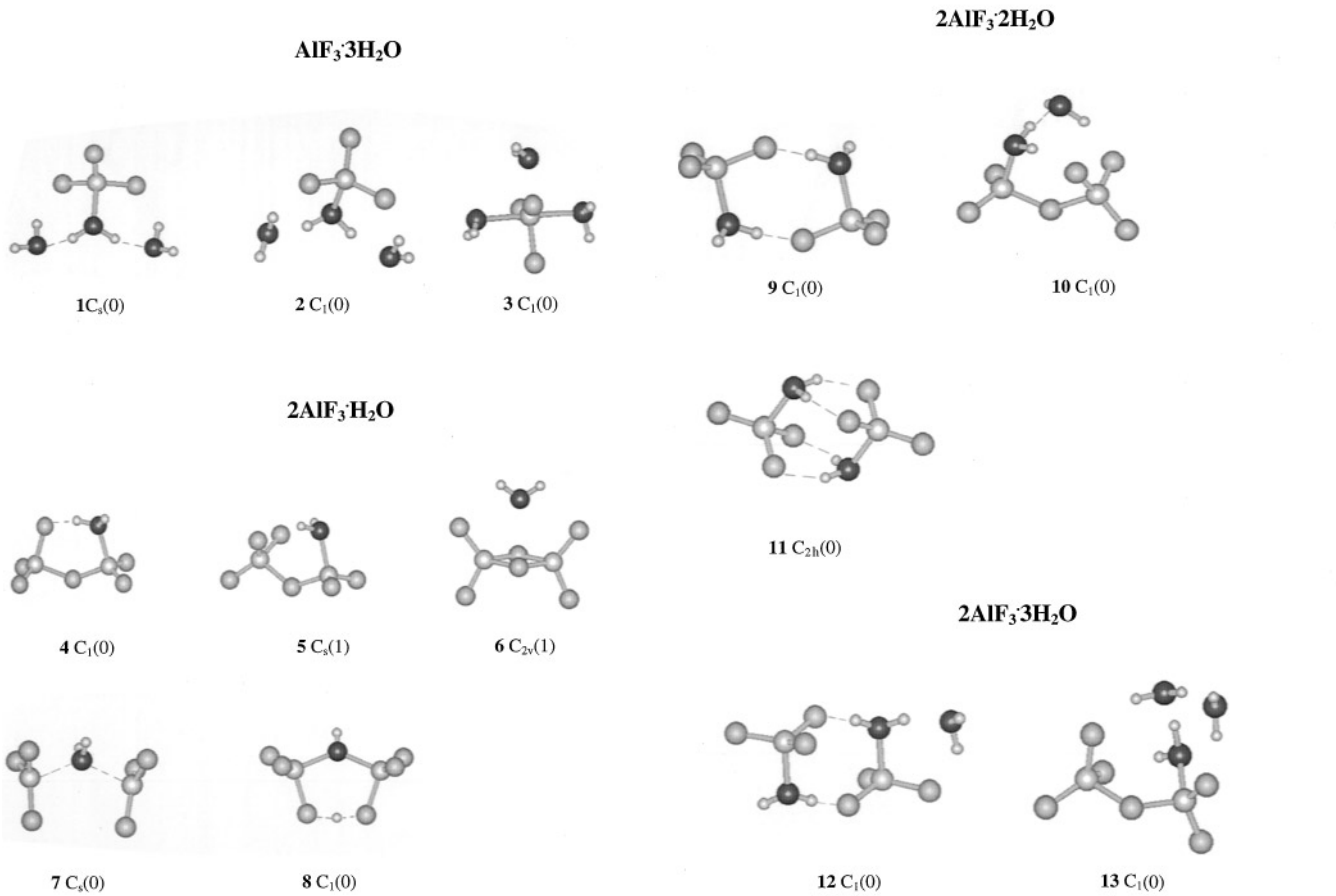

FIG. 8. Structure models used for the complexes $AlF_3 \cdot 3H_2O$, $2AlF_3 \cdot H_2O$, $2AlF_3 \cdot 2H_2O$, and $2AlF_3 \cdot 3H_2O$. Values in parentheses indicate the nature of the stationary point: (0), local minimum; (1), first order saddle point.

two Al–F–Al– bridges (cf. structure 6) does not result in stable structures.

These findings are supported by the calculations of larger structure models consisting of two AlF_3 and two or three H_2O molecules. They result in either $\{AlF_3–OH_2\}$ subunits connected by two or more hydrogen bridges (Fig. 8, structures 9, 11, 12) or $\{F_3AlFAlF_2–OH_2\}$ units stabilized by hydrogen bridges (structures 10, 13). The energy differences between the three local minima obtained for $2AlF_3–2H_2O$ (structures 9–11) and for $2AlF_3–3H_2O$ (structures 12, 13) appear to be extremely low (see Table 1). At the DFT(B3LYP)/6-31+G* level structures 10 and 12 represent the global minima. That means that one H_2O molecule is sufficient to split one of the two –Al–F–Al– bridges of the Al_2F_6 dimer. However, at least three water molecules are necessary to split both bridges.

The complex interaction energies ΔE of all *global minima* are summarized together with the zero-point vibrational energies, the basis set superposition errors, and the reaction enthalpies at 0 K in Table 2.

Figure 9 gives an overview on calculated harmonic vibrational frequencies of all identified global and local minima of $(AlF_3)_n(H_2O)_m$ complexes along with the frequencies of the subunits H_2O, $(H_2O)_2$, $(H_2O)_3$, AlF_3, and $(AlF_3)_2$, allowing molecular and intermolecular modes to be more easily assigned.

One of the main conclusions from these calculations, which are of general relevance and especially relevant here for the solid state ESR experiments, is the following: Whenever water is present, the formation of a strong Al–O– bond has to be expected. Moreoever, two fluoride bridges between two aluminum atoms will be split if enough water molecules are available. As a consequence, both the stable $AlF_3–OH_2$ complex and the $\{F_3AlFAlF_2–OH\}$ unit with a cyclic $\{AlFAlO\}$ arrangement could be identified as subunits in all model structures discussed in this paper.

TABLE 1

Calculated Total Energies (E_{tot}) and Relative Energies (ΔE^{rel}) of Structure Models for $(AlF_3)_n \cdot (H_2O)_m$ Complexes (DFT (B3LYP/6-31+G* level))

Molecule/complex	E^{tot} (au)	ΔE^{rel} (kJ/mol)
AlF_3–$3H_2O$, 1 (C_s)	− 771.576809	0.0
AlF_3–$3H_2O$, 2 (C_1)	− 771.576152	1.7
AlF_3–$3H_2O$, 3 (C_1)	− 771.557004	52.0
$2AlF_3$–H_2O, 4 (C_1)	− 1160.943580	0.0
$2AlF_3$–H_2O, 5 (C_s)	− 1160.940634	7.7
$2AlF_3$–H_2O, 6 (C_{2v})	− 1160.920080	61.7
$2AlF_3$–H_2O, 7 (C_1)	− 1160.896415	123.8
$2AlF_3$–H_2O, 8 (C_1)	− 1160.926332	45.3
$2AlF_3$–$2H_2O$, 10 (C_1)	− 1237.397395	0.0
$2AlF_3$–$2H_2O$, 9 (C_2)	− 1237.397338	0.2
$2AlF_3$–$2H_2O$, 11 (C_{2h})	− 1237.392453	13.0
$2AlF_3$–$3H_2O$, 12 (C_1)	− 1313.845924	0.0
$2AlF_3$–$3H_2O$, 13 (C_1)	− 1313.84210	10.0

5. DISCUSSION

Generally, two methods for the preparation of amorphous aluminum fluoride are in use: (i) Thermal dehydration processes, which start from $AlF_3 \cdot 3H_2O$ (2), lead to amorphous AlF_3 after the primary water content is given up and before the catalytical active β-AlF_3 phase is formed. (ii) Thermal evaporation of crystalline or amorphous and nominally water-free AlF_3, followed by condensation at a target which is held at temperatures below 200°C, also results in amorphous AlF_3.

The disorder of amorphous AlF_3 should be caused mainly by distributions of F–Al–F bond angles and to a less extent by Al–F bond lengths and the mutual orientation of $\{AlF_6\}$ polyhedra.

Experimental Findings Concerning the Influence of Water at the Reorganization of Amorphous AlF_3

The typical X-band ESR spectrum of amorphous AlF_3 doped with Mn^{2+} ions deposited under vaccum conditions is shown in Fig. 2a. The value of the ^{55}Mn–hyperfine coupling constant, 9.8 mT, covers the range expected for fluorine coordination of Mn^{2+} ions (see for comparison Fig. 1). The unresolved ^{55}Mn–^{19}F–shfs together with the line widths of the hyperfine transitions are typical for Mn^{2+}-doped amorphous fluorides (9). The hygroscopic properties of amorphous AlF_3 can be demonstrated unambiguously by FT-IR microscopic measurements, given in Fig. 2. Even FT-IR experiments with freshly prepared amorphous samples exposed to air yield essentially the spectral pattern of α-$AlF_3 \cdot 3H_2O$. It can be expected that the hydrated amorphous solid has remarkedly disordered surface structures. However, neither structures nor energies (stabilities) of intermediates formed at the surface or in the vapor phase have been available until now.

TABLE 2

Total Energies E^{tot} (au), Zero Point Vibrational Energies, ZPVE (au), Interaction Energies, ΔE (kJ/mol), Basis Set Superposition Errors, BSSE (kJ/mol), and Reaction Enthalpies at O K $\Delta_R H^0$ (kJ/mol) of Several AlF_3- and H_2O-Containing Molecules (Global Minima) Calculated at the DFT(B3LYP)/6-31+G* Level

Molecule/complex	E^{tot} (au)	ZPVE (au)	ΔE (kJ/mol)	ΔZPVE (kJ/mol)	BSSE (kJ/mol)	ΔH^0 (kJ/mol)
H_2O, C_{2v}	− 76.422572	0.021089	—	—	—	—
$2H_2O$, C_s	− 152.855412	0.046159	− 26.96	10.45	4.79	− 11.72
$3H_2O$, C_s	− 229.285905	0.070522	− 47.76	19.05	8.95	− 19.76
AlF_3, D_{3h}	− 542.205980	0.007636	—	—	—	—
$2AlF_3$, D_{2h}	− 1084.484917	0.017637	− 191.5	6.2	9.5	− 175.79
AlF_3–H_2O, C_s	− 618.676626	0.033043	− 126.2	11.34	9.2	− 105.7
AlF_3–$2H_2O$, C_1	− 695.128739	0.058839	− 203.78	23.70	16.60	− 163.48
AlF_3–$3H_2O$, 1 (C_s)	− 771.576809	0.084264	− 270.72	35.07	23.39	− 212.26
$2AlF_3$–H_2O, 4 (C_1)	− 1160.943580	0.042882	− 286.30	17.2	16.98	− 252.20
$2AlF_3$–$2H_2O$, 10 (C_1)	− 1237.397395	0.068778	− 368.33	29.74	26.45	− 312.14
$2AlF_3$–$3H_2O$, 12 C_1	− 1313.845924	0.093702	− 436.48	39.80	32.82	− 363.86

Notes: The complex binding energies ΔE of $(AlF_3)_n(H_2O)_m$ complexes are calculated according to: $\Delta E = E^{tot} - n\,E^{tot}_{AlF_3} - m E^{tot}_{H_2O}$, and $\Delta H^0 = \Delta E +$ BSSE + ΔZPVE.

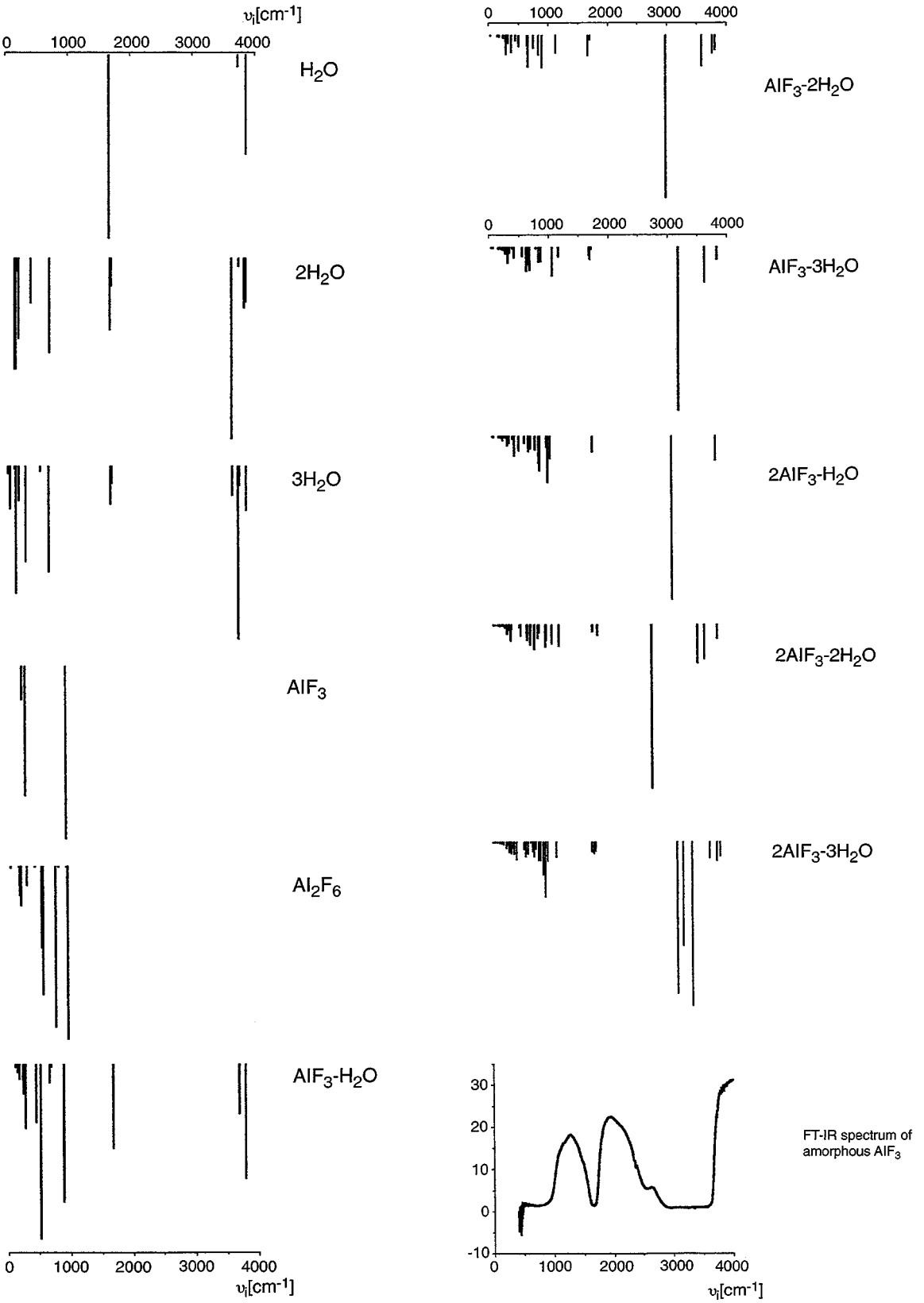

FIG. 9. Calculated IR spectra of all identified global minima of the $(AlF_3)_n(H_2O)_m$ complexes considered presently, as well as the subunits H_2O, $(H_2O)_2$, $(H_2O)_3$, AlF_3, and $(AlF_3)_2$ (IR intensities in km/mole). Calculations have been performed at the DFT(B3LYP)/6-31+G* level.

Thermal treatment of vapor-deposited amorphous AlF_3 under different atmospheres and temperatures (cf. Fig. 4–7) gave evidence for the crucial role of water traces on crystallization processes of the amorphous AlF_3-matrix for temperatures up to 400°C. The formation of crystalline regions doped with $\{MnF_6\}$ point defects is indicated by the spectral resolution of both the ^{55}Mn–hfs (9.8 mT) and the ^{55}Mn–^{19}F–shfs (2.4 mT) in the ESR spectra and by the pattern of X-ray powder diffractograms (Fig. 4, 5). The values obtained for the hyperfine and superhyperfine couplings are in excellent agreement with those obtained for Mn^{2+}-doped crystalline α-AlF_3 (Fig. 1).

A reorganization of amorphous water-free AlF_3 into at least local crystalline water-free AlF_3 takes place *only* in the presence of water, which mediates locally alternating hydration/dehydration processes accompanied by structural rearrangements. The paramagnetic probe ion Mn^{2+} sensitively allows a local view of structural rearrangements and offers the possibility of attempting even molecular interpretations of reorganization processes.

The large ^{55}Mn-shf coupling constant, 9.8 mT in both amorphous and crystalline AlF_3, implies a fluorine coordination of Mn^{2+} ions in both phases. An oxygen coordination of Mn^{2+} ions as result of local reactions with water molecules would lead to a distinctly diminished ^{55}Mn–hyperfine coupling constant (11). Following that, a *periodic reaction with water molecules* must occur, with water being the catalytic agent for the reorganization of amorphous AlF_3. Local hydration/dehydration processes imply the reaction of water molecules with aluminum fluoride. The knolwedge of structures and stabilities of molecular intermediates between H_2O and AlF_3 molecules in the gas phase or at the surface should be helpful for an understanding of hydration and dehydration processes at a molecular level.

Molecular Models for Possible Intermediates in Structural Reorganization Processes of Amorphous AlF_3

Because experimental evidence of molecular intermediates in the gas phase or at the surface is difficult and until now not available, quantum chemical approaches were the methods of choice. As results, conclusions regarding structures, stabilities, and frequencies of harmonic vibrations for several structure models (discussed in Sect. 4) can be derived.

Ab initio calculations of the complexes $(AlF_3)_n(H_2O)_m$ (n: 1,2; m: 1–3) at the DFT(B3LYP)/6-31+G* level (Fig. 8) implied the formation of *one* essential and stable intermediate subunit, AlF_3–OH_2, which appears to be the main structural subunit of almost all models given in Fig. 8. Moreover, Al–F–Al– bonds experience a splitting in the presence of water molecules, which was shown with the help of model calculations of intermediates consisting of two AlF_3 and one H_2O molecules (Fig. 8, Table 2). Even this subunit (Fig. 8, structure 4) can be recognized as having been taken into account in larger molecular models (structures 10, 13). The calculated harmonic vibrational frequencies (Fig. 9) for every chosen structure model reflect details of the experimentally registered FT-IR spectrum of amorphous AlF_3. Only those models large enough to simulate approximately the first steps of a hydrogen-bridged network yield frequencies reproducing details of the experimentally observed spectra, such as the shoulder in the range of 2500 cm^{-1}.

A generalized and simplified scheme (Fig. 10) shows the key role of water and gaseous intermediates in the vapor phase or at the surface for reorganization and doping processes. The influence of thermal energy on the formation and decomposition of the aluminum fluoride hydrates as a basic effect is not explicitly demonstrated in this scheme (Fig. 10). The driving forces for the decomposition and reorganization of the remaining AlF_3 can be identified as (i) the reaction between free or weakly bonded H_2O (OH^-) and active amorphous AlF_3 in the neighborhood, (ii) the thermally stimulated reorganization of AlF_3, and (iii) the transport of entropy by liberation of H_2O.

6. CONCLUSIONS

ESR spectroscopic measurements have unambiguously demonstrated that Mn^{2+} ions are suitable spin probes for the indication and characterization of amorphous or local crystalline regions in fluoride matrices. Crystalline regions in the AlF_3 matrix are manifested by the appearance of the ^{55}Mn–^{19}F– superhyperfine structure in the ESR spectrum, which shows without any doubt the existence of MnF_6^{4-} polyhedra. Starting from amorphous samples this

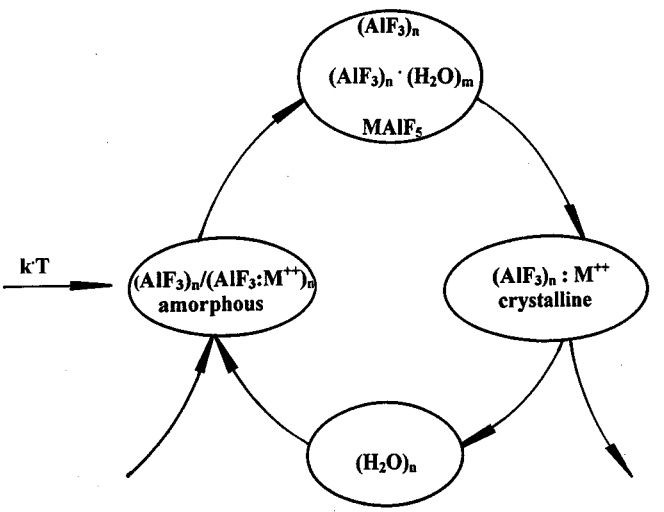

FIG. 10. Depiction of the key role of water during thermally induced reorganization processes of doped aluminum fluorides.

^{55}Mn–^{19}F–shfs, and therewith the reorganization to local crystalline regions, can only be resolved if a distinct partial pressure of water is available during the application of thermal energy. The ESR information about the local structures obtained here is unique and cannot be achieved in detail by other methods, like diffraction or thermal methods. These experimental findings include periodic participation of water molecules in transformation processes, that is hydration/dehydration reactions. Nonperiodic reactions, e.g., only hydration processes, should result in the formation of Mn–O bonds, observable by a diminished ^{55}Mn–hf coupling constant (11), and the absence of, or presence of only partially resolved, ^{55}Mn–^{19}F–shfs.

Moreover, the experimental results support the idea of intermediates of AlF_3 and H_2O existing at least in the surface region of amorphous aluminum fluoride and/or in the vapor phase.

DFT(B3LYP)/6-31+G* calculations of several structure models of the complexes $(AlF_3)_n(H_2O)_m$ (n: 1,2; m: 1–3) resulted in first and acceptable ideas of structures, energetical stabilities, and vibrational frequencies of hydrated AlF_3. The calculated strength of the Al–O bond, resulting in the stable AlF_3–OH_2 subunit, as well as the favored splitting of Al–F–Al bonds by H_2O molecules are able to explain the immediate and spontaneous hydration of freshly prepared amorphous AlF_3. Independent of the size of the model complexes, stable substructures like $\{AlF_3$–$H_2O\}$ and $\{F_3AlFAlF_2$–$OH_2\}$ can be recognized in all optimized structure models.

The calculated equilibrium structures (global minima at the potential energy surfaces) acceptably model the gaseous and surface complexes between AlF_3 and H_2O molecules. They represent steps toward modeling the formation of solid $AlF_3 \cdot 3H_2O$ at a molecular level.

ACKNOWLEDGMENTS

G.S. gratefully acknowledges Prof. Dr. R. Stösser for helpful discussions and continuous support. Special thanks go to Dr. U. Bentrup and W. Winkler for thermoanalytical and IR measurements, to S. Hoffmann for many vapor deposition and ESR experiments, and to Dr. A. Dummer and Dr. M. Krossner for several quantum chemical calculations. The Deutsche Forschungsgemeinschaft and the Konrad – Zuse Zentrum für Informationstechnik Berlin are kindly acknowledged for financial support and computer time on the CRAY-YMP, respectively.

REFERENCES

1. (a) A. E. Comyns, Ed. "Fluoride glasses." J. Wiley & Sons, New York, 1989. (b) A. Heß, E. Kemnitz, A. Lippitz, W. E. S. Unger, and D.-H. Menz, *J Catal.* **148,** 270 (1994).
2. (a) R. Stößer, G. Scholz, and M. Päch, *J. Solid State Chem.* **116,** 249 (1995). (b) D.-H. Menz, L. Kolditz, K. Heide, C. Schmidt, Ch. Kunert, Ch. Mensing, H.G.v. Schnering, and W. Hönle, *Z. Anorg. Allg. Chem.* **551,** 231 (1987). (c) D.-H. Menz, Ch. Mensing, W. Hönle, and H. G. v. Schnering, *Z. Anorg. Allg. Chem.* **611,** 107 (1992). (d) D.-.H. Menz, A. Zacharias, and L. Kolditz, *J. Therm. Anal.* **33,** 811 (1998).
3. D.-H. Menz, G. Scholz, D. Becker, and M. Binnewies, *Z. Anorg. Allg. Chem.* **620,** 1976 (1994).
4. (a) G. Scholz, R. Stösser, and J. Bartoll, *J. Phys. Chem.* **100,** 6518 (1996). (b) M. Krossner, G. Scholz, and R. Stösser, *J. Phys. Chem.* **101,** 1555 (1997).
5. A. D. Becke, *J. Chem. Phys.* **98,** 5648 (1993).
6. M. J. Frisch, G. W. Trucks, H. B. Schlegel, P. M. W. Gill, B. G. Johnson, M. A. Robb, J. R. Cheeseman, T. Keith, G. A. Petersson, J. A. Montgomery, K. Raghavachari, M. A. Al-Laham, V. G. Zakrzewski, J. V. Ortiz, J. B. Foresman, C. Y. Peng, P. Y. Ayala, W. Chen, M. W. Wong, J. L. Andres, E. S. Replogle, R. Gomperts, R. L. Martin, D. J. Fox, J. S. Binkley, D. J. DeFrees, J. Baker, J. J. P. Stewart, M. Head-Gordon, C. Gonzalez, and J. A. Pople, Gaussian 94, Rev. B.3, Gaussian, Inc., Pittsburgh PA, 1995.
7. S. Hoffmann, Diploma thesis, Humboldt University of Berlin, 1996.
8. R. Stösser, G. Scholz, *Appl. Magn. Reson.* **12,** 167 (1997).
9. (a) C. Legein, J. Y. Buzare, and C. Jacoboni, *J. Non-Cryst. Solids* **161,** 112 (1993). (b) J. M. Dance, J. J. Videau, and J. Portier, *J. Non-Cryst. Solids* **86,** 88 (1986). (c) L. D. Bogomolova, V. A. Jachkin, N. A. Krasilnikova, V. L. Bogdanov, E. B. Fedorushka, and V. D. Khalilev, *J. Non-Cryst. Solids* **125,** 32 (1990).
10. G. Scholz, R. Stösser, S. Sebastian, E. Kemnitz, and J. Bartoll, *J. Phys. Chem. Sol.*, 1998, submitted.
11. (a) A. F. M. Y. Haider and A. Edgar, *J. Phys. C* **13,** 6239 (1980). (b) J. J. Davies, S. R. P. Smith, and J. E. Wertz, *Phys. Rev.* **178,** 608 (1969).